## Crustal and upper mantle structure beneath south-western margin of the Arabian Peninsula from teleseismic tomography

(Article begins on next page)

22 May 2024

## Geochemistry, Geophysics, Geosystems

# Crustal and upper mantle structure beneath south-western margin of the Arabian Peninsula from teleseismic tomography

**Félicie Korostelev[1,2], Clémence Basuyau[3], Sylvie Leroy[1,2], Christel Tiberi[4], Abdulhakim Ahmed[1,2,5], Graham W. Stuart[6], Derek Keir[7], Frédérique Rolandone[1,2], Ismail Al Ganad[8], Khaled Khanbari[9], and Lapo Boschi[1]**

[1]Sorbonne Universités, UPMC Univ Paris 06, UMR 7193, Institut des Sciences de la Terre Paris, Paris, France, [2]CNRS, UMR 7193, Institut des Sciences de la Terre Paris, Paris, France, [3]University Paris Diderot, Institut de Physique du Globe de Paris, Paris, France, [4]CNRS Géosciences Montpellier, Montpellier, France, [5]Seismological and Volcanological Observatory Center, Dhamar, Yemen, [6]School of Earth and Environment, University of Leeds, Leeds, UK, [7]National Oceanography Centre Southampton, University of Southampton, Southampton, UK, [8]Yemen Geological Survey and mineral Resources Board, Sana'a, Yemen, [9]Sana'a University, Yemen Remote Sensing and GIS Center, Sana'a, Yemen

**Abstract** We image the lithospheric and upper asthenospheric structure of western continental Yemen with 24 broadband stations to evaluate the role of the Afar plume on the evolution of the continental margin and its extent eastward along the Gulf of Aden. We use teleseismic tomography to compute relative $P$ wave velocity variations in south-western Yemen down to 300 km depth. Published receiver function analysis suggest a dramatic and localized thinning of the crust in the vicinity of the Red Sea and the Gulf of Aden, consistent with the velocity structure that we retrieve in our model. The mantle part of the model is dominated by the presence of a low-velocity anomaly in which we infer partial melting just below thick Oligocene flood basalts and recent off-axis volcanic events (from 15 Ma to present). This low-velocity anomaly could correspond to an abnormally hot mantle and could be responsible for dynamic topography and recent magmatism in western Yemen. Our new $P$ wave velocity model beneath western Yemen suggests the young rift flank volcanoes beneath margins and on the flanks of the Red Sea rift are caused by focused small-scale diapiric upwelling from a broad region of hot mantle beneath the area. Our work shows that relatively hot mantle, along with partial melting of the mantle, can persist beneath rifted margins after breakup has occurred.

## 1. Introduction

The Afar triple junction, where the Red Sea, East African, and Gulf of Aden rifts intersect (Figure 1), is a key region to understand how continental breakup occurred under the influence of a plume and abnormally hot mantle [e.g., *Bastow et al.*, 2011]. Many seismological studies have been carried out in north-east Africa and Arabia to determine the depths of the Moho [e.g., *Ahmed et al.*, 2013; *Mechie et al.*, 2013] and to image upper mantle structure and understand regional geodynamics [e.g., *Bastow et al.*, 2005; *Benoit et al.*, 2003, 2006; *Montagner et al.*, 2007; *Zhao*, 2007; *Sicilia et al.*, 2008; *Chang and Van der Lee*, 2011; *Koulakov*, 2011] and how it is connected with global mantle flow [e.g., *Montelli et al.*, 2006; *Boschi et al.*, 2007, 2008; *Forte et al.*, 2010; *Moucha and Forte*, 2011]. However, no previous study has the resolution in continental Yemen on the Gulf of Aden margin due to the lack of seismic stations. Surface wave studies [e.g., *Debayle et al.*, 2001; *Sebai et al.*, 2006; *Montagner et al.*, 2007; *Sicilia et al.*, 2008; *Chang et al.*, 2011; *Chang and Van der Lee*, 2011] lack sufficient lateral resolution to image the detail of lithospheric and uppermost mantle structures.

The YOCMAL project (Young Conjugate Margins Laboratory) deployed 23 broadband stations in a network running from the Red Sea margin to Aden city, passing through the Yemeni highlands and Sana'a city (Figure 2). Using classical teleseismic tomography [*Aki et al.*, 1977] on recordings from these stations together with a permanent Geofon station (DAMY), we image the relative velocity variations of $P$ waves in the crust and upper mantle down to 300 km depth. We thus: (1) characterize the lithospheric structure of the rifted margins of the Gulf of Aden and Red Sea system of western Yemen and (2) locate the presence of asthenospheric upwellings in the region and their interaction with the lithosphere.
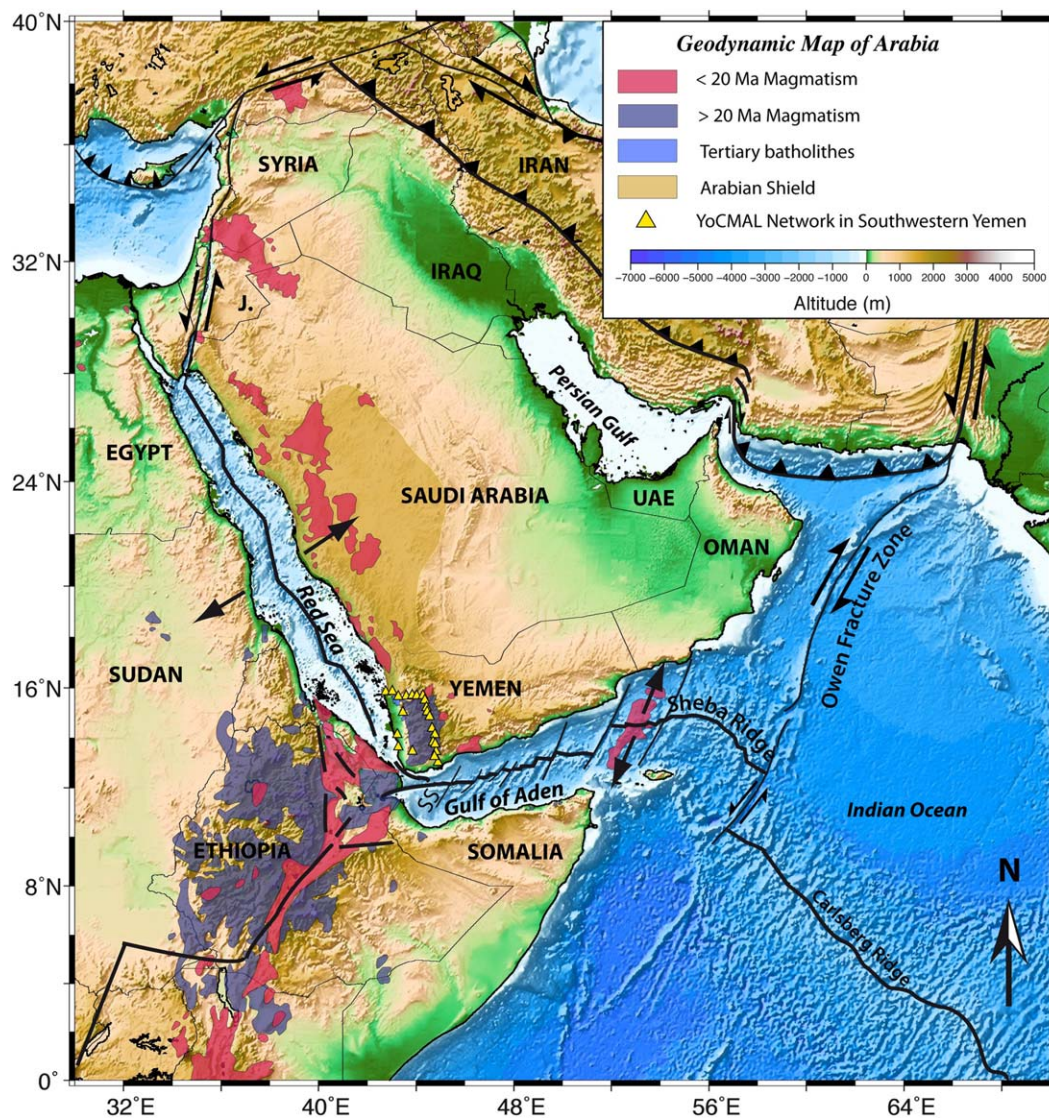
**Figure 1.** Geodynamic map of Arabia. Yellow triangles are for YOCMAL Network stations in southwestern Yemen. The magmatism older than 20 Ma is represented in purple, whereas the younger magmatism is in pink [modified from *Davison et al.*, 1994]. J.: Jordan, UAE: United Arab Emirates, SS.: Shukra el Sheik Fracture Zone.

## 2. Geodynamic Setting

The Red Sea and Gulf of Aden rifts are connected to the East African rift at the Afar triple junction, in the "Horn of Africa." In the Afar triple junction region, the presence of flood basalts [e.g., *Baker et al.*, 1996; *Hofmann et al.*, 1997; *George et al.*, 1998] and an abnormally low-velocity upper mantle anomaly [e.g., *Debayle et al.*, 2001; *Bastow et al.*, 2005] could be due to the presence of a mantle plume (Figure 1). Around 35 Ma ago, the current rift system began to open, under the influence of the Afar plume [e.g., *Leroy et al.*, 2012]. The flood basalts of Ethiopia and Yemen are the signatures of voluminous eruptions produced during the Paleogene [*Ebinger and Sleep*, 1998] with highest eruption rates at 31 Ma [*Baker et al.*, 1996; *Hofmann et al.*, 1997; *George et al.*, 1998]. A renewed phase of volcanism took place 24 Ma ago that corresponds with the synchronous appearance of basaltic dikes and gabbros along the Red Sea, from Afar and Yemen to northern Egypt. From 25 to 16 Ma, a series of basaltic, trachytic, and rhyolitic dikes were emplaced along the Red Sea margins [*Zumbo et al.*, 1995], at the same time as emplacement of large granitic batholiths (Jabal Hufash and Jabal Bura, see Figure 2). These granites are oriented north-south [*George et al.*, 1998] and located at the border of the Great Escarpment, a 1000 km long sudden change in altitude, from 200 m on the west in
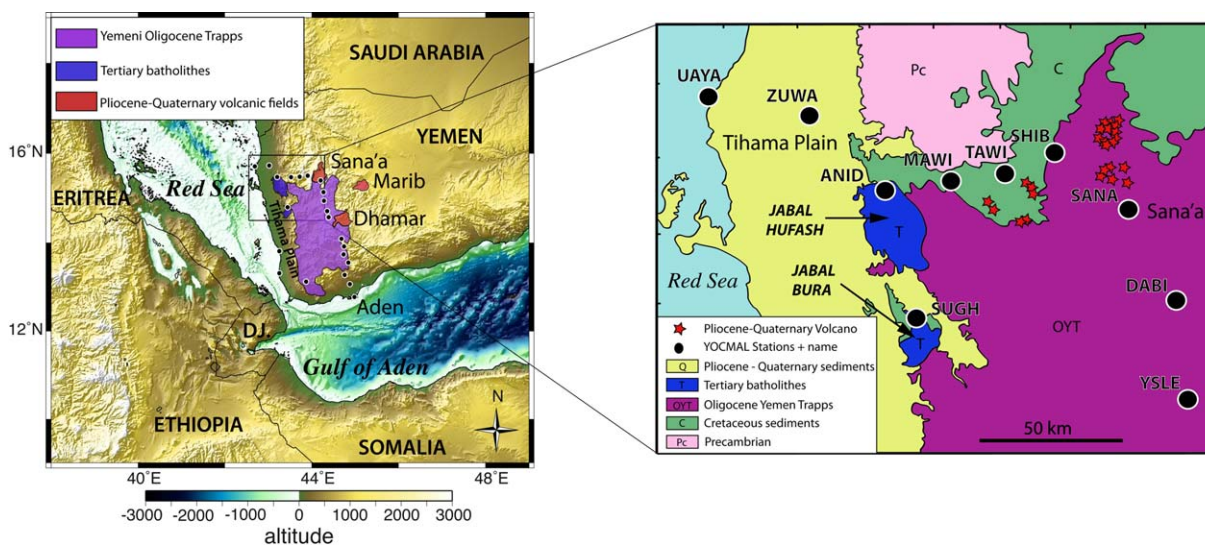
**Figure 2.** (a) Topographic map of South-western Yemen. The Yemeni highlands, above 1000 m high, are mainly constituted by basaltic traps. These basalts are 3 km thick. The volcanic Pliocene to present-day volcanic fields of Sana'a and Dhamar are represented in red. Jabal Hufash and Jabal Bura Tertiary batholiths are in blue [modified from *Davison et al.*, 1994]. Black dots are for YOCMAL seismological stations. (b) Geological sketch of the northern part of our study area. Red stars are for Pliocene-Quaternary volcanoes. The batholiths are located along the Great Escarpment, which runs parallel to the Red Sea margin and the Tihama Plain. Left of the Great Escarpment, altitudes are below 200 m.

the Tihama Plain, to more than 1000 m in the Yemeni highlands. In addition, syn-rift (30–16 Ma) basaltic flows dipping toward the sea (seaward dipping reflectors–SDRs) have been imaged under the Tihama Plain [*Davison et al.*, 1994]. In the Red Sea, a second phase of opening began 14 Ma ago synchronous with the formation of the Dead Sea transform fault to the north. This phase is accompanied by increased extension rates and rift-flank uplift [*Courtillot et al.*, 1999].

From 12 Ma to present, magmatic provinces developed within a 2500 km radius of Afar and south-western Yemen as far away as western Saudi Arabia, Jordan, and northern Syria, [*Zumbo et al.*, 1995; *Bertrand et al.*, 2003; *Coulié et al.*, 2003], see Figure 1. Recent magmatism has occurred offshore in the ocean-continent transition of the Eastern Gulf of Aden margin [*Lucazeau et al.*, 2009; *Autin et al.*, 2010; *Watremez et al.*, 2011], off-axis Sheba ridge [*d'Acremont et al.*, 2010], and below the southern Oman continental margin [*Basuyau et al.*, 2010] (Figure 1). The increased magmatism caused by extension above a plume was first thought to stop at the Shukra al Sheik fracture zone [e.g., *Hébert et al.*, 2001], but these recent results indicate that the limit could be further east (Figure 1), as proposed by *Leroy et al.* [2010a].

The Gulf of Aden is characterized by two stretched continental margins systems: nonvolcanic margins in the east and volcanic margins in the west near the Afar triple junction. The volcanic margins are associated with syn-rift SDRs up to 5 km thick [*Tard et al.*, 1991; *Leroy et al.*, 2012]. SDRs are also sparsely found in the east especially at the ocean-continent transition [*Autin et al.*, 2010; *Leroy et al.*, 2010b], but no syn-rift volcanism has been found east of the longitude 46°E, see Figure 1 [*Leroy et al.*, 2012]. The study region is near the edge of the African superplume, as shown by large-scale global tomographic models [e.g., *Debayle et al.*, 2001; *Sebai et al.*, 2006; *Boschi et al.*, 2007, 2008] and by petrologically derived temperature estimates of the mantle [*Rooney et al.*, 2012; *Rolandone et al.*, 2013].

## 3. Data

Data have been collected from 23 temporary broadband stations deployed from March 2009 to March 2010 (YOCMAL project), and from one permanent station (DAMY, Geofon). The network extends from the Red Sea margin to the Gulf of Aden margin, passing through the Yemeni highlands (Figure 2). The sensors deployed were Guralp 40T (sampling rate 50 sps, 30 s natural period), 6TD (sampling rate 40 sps, 30 s natural period), and ESPD (sampling rate 40 sps, 60 s natural period). This network configuration allows imaging structures with a high resolution, and down to 300 km depth (the surface extent of our network). We
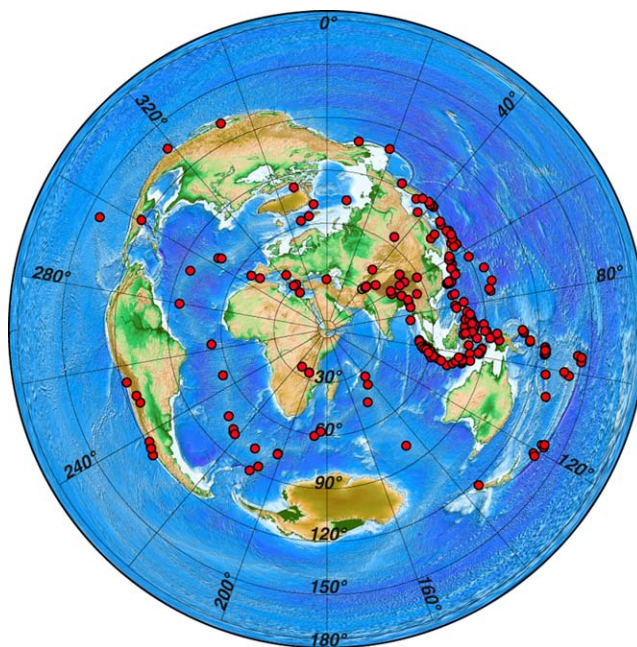
**Figure 3.** Azimuthal distribution of the events used on our study.

selected 200 teleseismic events with clear first *P* wave arrivals from earthquakes with magnitude $\geq 5.5$. Among them, 142 events arrived as P, 35 events as PP, and 23 events as PKP (Figure 3), and were picked on consistent peaks in the first cycle. We used 2456 delay times calculated relative to the IASP91 Earth model [*Kennett and Engdahl*, 1991]. For each residual, a picking error was assigned within the range $\pm 0.05$ to $\pm 0.2$ s. As the events registered come mostly from east/northeast and have a range of epicentral distances, the rays are crossing, and we expect our best resolution in this direction.

## 4. Method

Our delay time residuals were inverted using the ACH teleseismic tomography method first used by *Aki et al.* [1974], then developed by *Weiland et al.* [1995], *Zeyen and Achauer* [1997], and *Jordan and Achauer* [1999]. As the inversion uses a 3-D iterative ray tracing at each step, the initial location of the parameterization nodes affects the inversion result [e.g., *Calò et al.*, 2008]. To reduce this problem, we averaged the results of four inversions with the same parameters of inversion, but with a meshing shifted by half a node (10 km) toward the east, north, and northeast compared with our initial reference model. This "Average Smooth model" technique smooths the local effects due to the meshing [*Evans and Achauer*, 1993]. The resulting velocity model is presented in Figure 4 as depth slices and in Figure 5 as depth cross sections.

Our network's dimensions are 360 km from North to South, 260 km from West to East, so our investigation depth (i.e., the depth until which we have resolution) is estimated to be ∼300 km [*Evans and Achauer*, 1993]. In our initial model, velocities are organized in successive horizontal layers of nodes, with an interpolation gradient between each of them [*Thurber*, 1983]. The minimum distance between two nodes horizontally is 20 km (i.e., the minimum distance between two stations). The node spacing is 40–100 km at the edges of the model. The initial model was the IASP91 reference Earth model. Ten levels of nodes were placed in depth between 0 and 500 km, so we have nine layers (nodes at 0, 30, 45, 70, 100, 150, 200, 250, 300, and 500 km depth). The thickness of the crust is important in the inversion process [e.g., *Zhao et al.*, 1994, 2006]. In our study, we use the receiver functions results of *Ahmed et al.* [2013] to compute a time correction for each station (Figure 6). This correction accounts for lateral variations in the crustal thickness, which are difficult to constrain by our teleseismic data alone; seismic velocity within the crust is treated as a free parameter in our inversion. The correction for each station is computed on the absolute residuals and is in the range −0.611 (for the station located on the thinnest crust) to 0.160 s (for the station located above the thicker crust). This allows a reduction in the propagation of crustal structure into the deeper layers of the velocity model.

The smoothing factor, which limits the short wavelength velocity variations, and the initial standard deviation associated with each node of the initial model for each of the nine iterations were chosen after a series of tests and are, respectively, 0.001 and 0.007 km s$^{-1}$. The smoothing value chosen is the same as *Tiberi et al.* [2008] and *Basuyau et al.* [2010]. Tests showed that the results are not significantly different for a standard deviation between 0.005 and 0.01 km s$^{-1}$. We tested these inversion parameters in order to get a stable model, choosing parameters that decrease the root mean square of

**Figure 4.** Final P wave velocity model obtained from inversion. Seismic stations are located with the black triangles. Note the color bar change between the first two layers and the other slices of the model, and the scale is saturated for the first layer.

**Figure 5.** Cross sections in the final P wave velocity model obtained from inversion. (a) Cross section along the Red Sea margin, (b) cross section along the Gulf of Aden margin, (c) cross section through the granitic intrusions of Jabal Hufash and Jabal Bura, (d) southwest-northeast cross section of the corner of Yemen.

**Figure 6.** Crustal correction applied for the stations. These corrections were computed from the crustal thickness obtained by receiver function analysis [*Ahmed et al.*, 2013].

residuals (RMS) through the inversion's nine iterations. The overall decrease of the RMS is 55% in the final model.

# 5. Results

## 5.1. Checkerboard Test

We use a checkerboard test to assess the resolution of our inversion. The synthetic checkerboard model consisted of rectangular velocity anomalies of +5% and −5% velocity variations at depths of 70, 200, and 300 km depth (Figure 7a). The size of the anomalies incr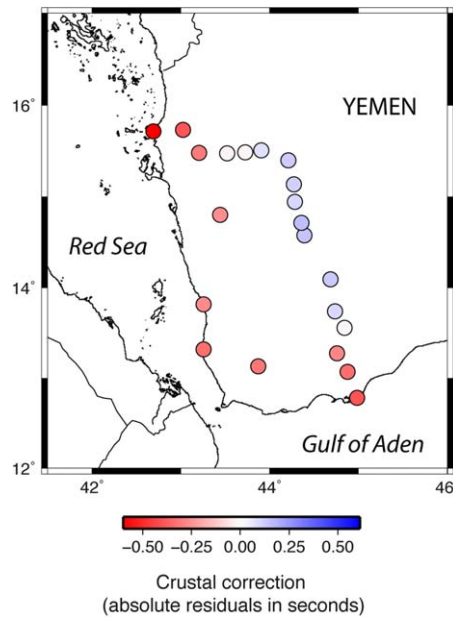eases around the edges as the method requires the nodes to be further apart at the edges of the model. We use the same inversion parameters (smoothing, standard deviation) as in our actual inversion.

The results of the checkerboard test (Figure 7b) show that at 70 km depth, due to the concentration of crossing rays under the stations, we have the best resolution, with ∼20% recovered amplitude. At 200 km depth, the crossing rays cover a larger area, so the anomalies are well retrieved. At 300 km depth, the eastern retrieved anomalies are much better constrained east of 44°E, due to the concentration of raypaths coming from the east. The Figure 7b shows the piercing points under our network at 300 km depth, at our maximum investigation depth. Below 300 km depth, the rays are too dispersed to give good resolution.

## 5.2. Crustal-Scale Structures

The thickness of the crust in our study area is estimated from receiver function analysis to be between 14 km at the coast and 35 km inland [*Ahmed et al.*, 2013]. The crust is represented by the first two layers of our model, and is characterized by the highest anomaly contrasts in *P* wave velocity, which have a range of
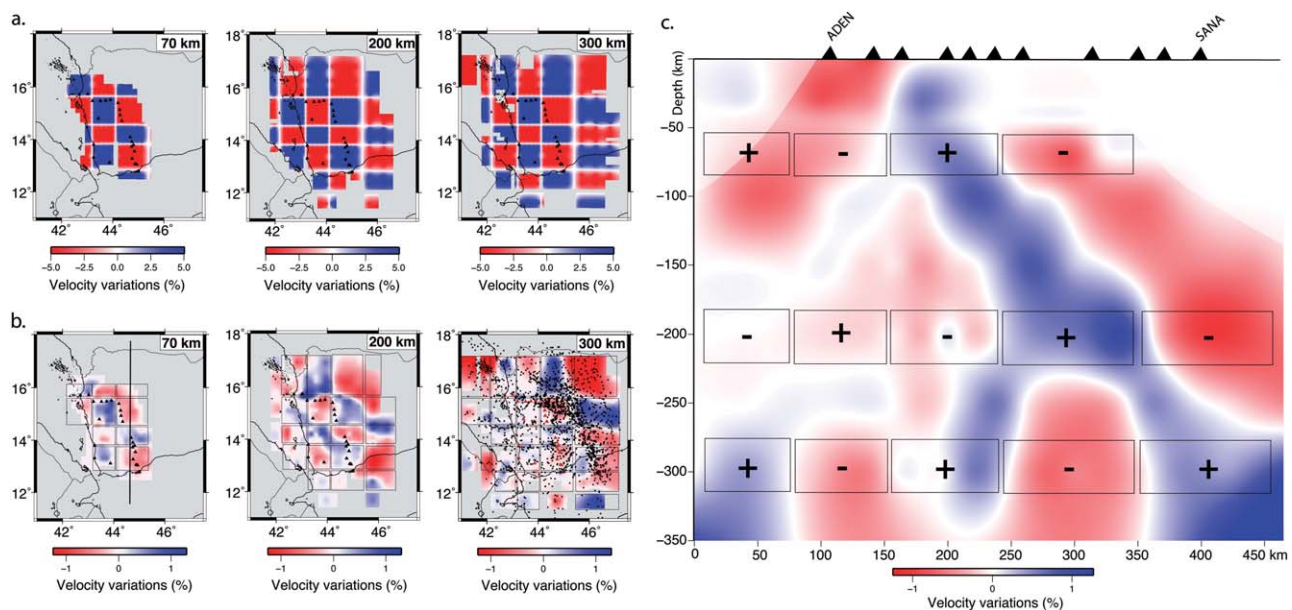


**Figure 7.** Checkerboard test for the inversion of seismological data. (a) Synthetic input model for *P* wave velocity, (b) depth slices at 70, 200, and 300 km through the retrieved velocity model, piercing points: impact points of the rays with the layer located at 300 km depth, (c) North-South cross section in the retrieved velocity model.
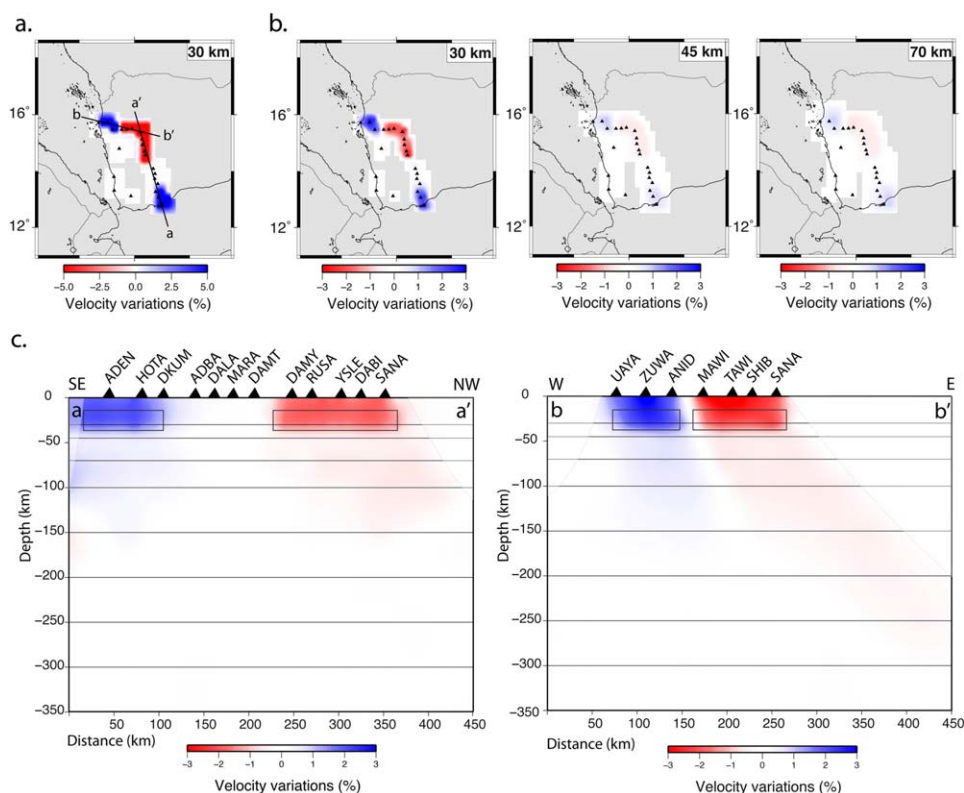
**Figure 8.** Synthetic test for the propagation of crustal signal. (a) Synthetic output model, (b) depth slices through the retrieved velocity model. (c) Cross sections of the Aden and Red Sea margins in the synthetic model.

±4% (Figures 4 and 5). These anomalies are related to geological structures observed at the surface. At 30 km depth, the strong low-velocity anomaly (−4%) beneath the center of our network (stations MAWI to DALA) correlates with the high topography of the plateau (>2000 m above sea level). We interpret this pattern as due to the thicker crust (>30 km) beneath the Yemeni highlands [*Ahmed et al.*, 2013].

Under stations located near the Red Sea (north-westernmost part of the network) and Gulf of Aden (southernmost part of the network) margins there are high-velocity anomalies above 30 km due to the thinner crust (<30 km). *Ahmed et al.* [2013] estimated the thickness of the crust to be ∼22 km in the coastal areas, and less than 14 km for the Red Sea margin. These high-velocity anomalies are located beneath SDRs, which is consistent with the emplacement of subaerial volcanic material during rifting [*Tard et al.*, 1991; *Davison et al.*, 1994; *Bastow and Keir*, 2011; *Leroy et al.*, 2012].

The high-velocity anomalies under the stations ANID and SUGH could be due to a thin crust as they are in the Red Sea coastal area, or to Tertiary granitic intrusions of Jabal Hufash and Jabal Bura, respectively [*Geoffroy et al.*, 2002], see Figure 2. The high-velocity anomaly corresponding to Jabal Hufash is imaged down to 45 km depth, which is slightly deeper than that of Jabal Bura (30 km depth). This can be explained by significant smearing due to the higher amplitude of the Jabal Hufash anomaly. There are lower velocities under the stations UAYA and ZUWA, on the Tihama plain (Figure 5b), probably due to ∼4000 m of low-velocity sediments [*El-Anbaawy et al.*, 1992; *Davison et al.*, 1994].

### 5.3. Upper Mantle Structures

The resulting upper mantle *P* wave anomalies are in the range of ±2%. The most striking pattern is a low-velocity anomaly located under the Yemeni highlands at 45 km depth, apparently dipping northeastward down to 300 km. It reaches its maximum amplitude at 70 km depth (east of the DAMY station) beneath the volcanic field of Dhamar (Figure 2), where there are two active volcanoes [*Manetti et al.*, 1991]. The northern part of this anomaly is located, at 70 km depth, under the volcanic field of Sana'a, which is also still active [*Manetti et al.*, 1991], see Figure 5.

There is a second low-velocity anomaly located under the south-western corner of Yemen and the stations MOKA and HAKI (Figures 5c and 5d). This low-velocity anomaly is nearly vertical and is recognized from the surface to 300 km. It is located just beneath the volcanic area of Jabal An Nar (Figure 5d), which was active during late Miocene, around 10 Ma, [*Manetti et al.*, 1991].

Even if we corrected the residuals from the crustal portion, our results are likely to include effects from Moho variations. This is because the corrections are based on receiver functions which display a strong trade-off between Moho depth and crustal velocity model. In addition, we took a 1-D velocity model to be consistent with the receiver functions study of *Ahmed et al.* [2013] and this can generate errors [*Martin and Ritter*, 2005]. The lack of detailed 3-D crustal information precludes us from going further with the crustal corrections than we have done. To estimate the resolution of our models in both the crust and the mantle, we proceed to synthetic tests. We test whether the low-velocity anomaly beneath the high plateau is dipping toward the northeast because of smearing along raypaths (Figure 3) in the next section. We investigate by means of synthetic tests whether: (1) the velocity variations observed in our resulting model are smearing downward into the mantle, (2) the low-velocity anomalies under the south-western corner of Yemen and under the high plateaus are artifacts, and whether we can determine at what depth they are located, and (3) the dipping low-velocity anomaly is related to the presence of partial melt or not.

## 6. Synthetic Tests and Presence of Melt

### 6.1. Propagation of Crustal Signal

We test the smearing with depth of a crustal anomaly (0–30 km) without a crustal correction by introducing a −5% anomaly around stations in the Yemeni Highlands and a +5% anomaly under the two continental margins (Figure 8a). The rest of the input model is laterally uniform. The results of the inversion of this synthetic model (Figures 8b and 8c) show that the velocity variations are well recovered in location but with 40% lower amplitude. Between 45 and 100 km depth, we can discern very low-amplitude anomalies (<0.5%), corresponding to a small amount of vertical smearing. At 100 km depth, we have a −1% anomaly under the Yemeni highlands. Approximately, half of this signal could be due to a smearing of the crust signal. No significant anomaly can be seen beneath 100 km depth. We conclude that crustal velocity anomalies do not propagate to deeper layers of our model and that there is an authentic low-velocity anomaly in the upper mantle. This test shows that the use of a crustal correction is relevant and is necessary to limit the extent of the propagation of crustal velocity structure into deeper layers of the model.

### 6.2. Low-velocity Anomalies Beneath South-Western Yemen

Using a synthetic input model, we simulate the resulting geometry of our final *P* wave model (see supporting information). We computed a series of tests (available in supporting information), and here we present the most relevant example. We first place a −5% anomaly under the three Yemeni volcanic fields of Sana'a, Dhamar, and Marib from the base of the crust down to 200 km depth. The other −5% anomaly is placed from the base of the crust to the base of our model, under the south-western corner of Yemen and southern Red Sea. Figure 9 shows the retrieved inversion image for a SW-NE profile (compare with the observed results in Figure 9c). Although the anomaly amplitudes within the crust are not retrieved, the dipping anomaly is quite well retrieved in the synthetic output model, as well as the low-velocity anomaly beneath Jabal An Nar volcanic field (Figure 9). This test shows that the dipping low-velocity anomaly under the Yemeni volcanic fields can be explained by a 220 × 260 km mantle upwelling between the base of the crust and 200 km depth. Moreover, the low-velocity anomaly beneath Jabal An Nar can be explained by a large zone of hotter mantle.

### 6.3. Presence of Partial Melt

Traveltime tomography gives the present state of the upper mantle in terms of velocity variations but it precludes any direct interpretation concerning their origin. Indeed, several factors, such as temperature, chemical composition, or anisotropy can affect the velocity of seismic waves [e.g., *Karato*, 1993; *Sobolev et al.*, 1996]. *Karato* [1993] demonstrates that a purely thermal origin leads to a linear relationship between P and S residuals with a slope of 2.9. *Gao et al.* [2004] proposed that a slope higher than 2.9 between P and S residuals for the same events highlights the presence of partial melting and several authors used the relationship to explain the presence of negative velocity anomalies in the upper mantle [e.g., *Bastow et al.*,
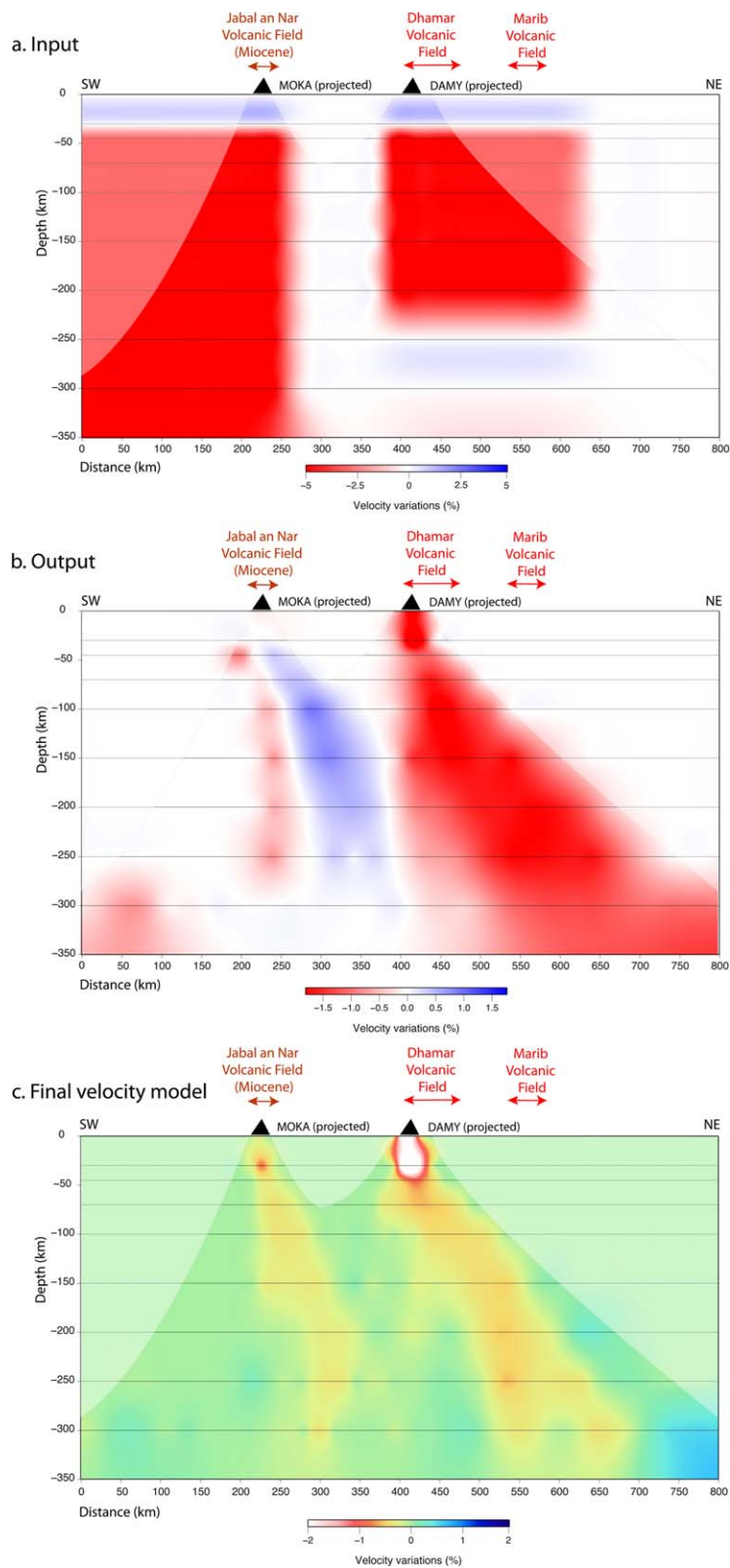
**Figure 9.** Synthetic test for two low-velocity anomalies under the South-western Yemen. (a) SW-NE cross section in the input model. (b) SW-NE cross section in the output model. (c) SW-NE cross section of the corner of Yemen from our final *P* wave velocity model.
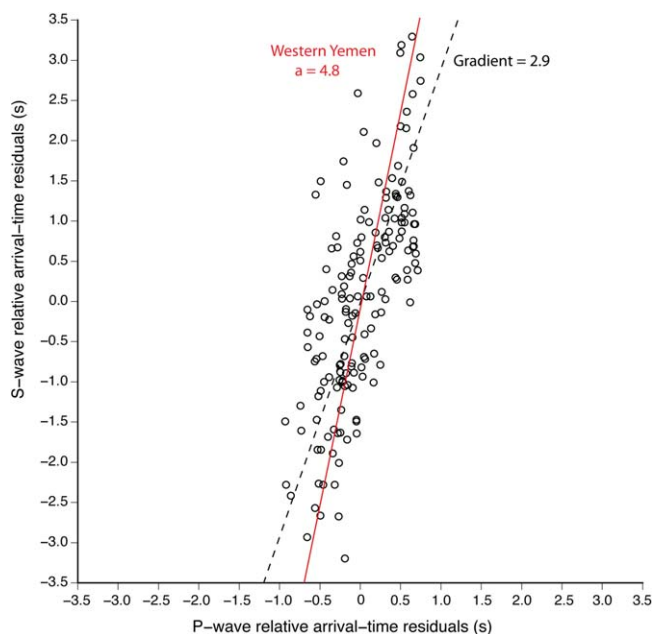
**Figure 10.** Plot of *P* wave versus *S* wave relative arrival-time residuals for all the stations and events coming from Northeast (Japan, China, Russia). The solid red line is the least squares fit to our data (with the slope of the line), and the dashed line is a slope of 2.9 (thermal effect only). Standard deviation is 0.31 for the best fit line and 0.36 for the 2.9 gradient.

2005; *Basuyau et al.*, 2010]. This method considers relative delay times, so that problems associated with amplitude recovery (e.g., due to differing numbers of traveltime observations and regularization levels) and other artifacts associated with the inversion procedure (i.e., parameterization and raypath accuracy) do not complicate the comparison of the data.

We thus selected the events coming from northeast (Russia, Japan, China), and picked the S arrival on the transverse component for stations located above the Yemeni Highlands, so that the rays chosen are passing through the northeastward dipping low-velocity anomaly. In Figure 10, following *Gao et al.* [2004], *Bastow et al.* [2005], and *Basuyau et al.* [2010], we plot S versus P relative traveltime residuals, and find out that our data are consistent with a slope >2.9, thus implying the presence of partial melt along the rays coming from northeast. The presence of Holocene volcanoes (in Sana'a, Dhamar, and Marib volcanic fields) on the surface helps support the idea that there is partial melt being created in the asthenosphere and intruding the lithosphere. Moreover, the isotopic signatures of the melts from the three volcanic fields suggest a strong asthenospheric component [*Manetti et al.*, 1991], which is consistent with our results.

## 7. Discussion

### 7.1. Crustal-Scale Structures

We produce a relative velocity model for the propagation of *P* waves down to 300 km beneath western Yemen. The low-velocity anomaly (∼−4%) located below the Yemeni highlands between 0 and ∼35 km corresponds to a region of 30–35 km thick crust [*Ahmed et al.*, 2013]. At 30 km depth, we observe a dramatic transition from very low to high velocities (−4% to +4%) under the coast of the Red Sea and Gulf of Aden. We interpret this sudden short length-scale (<40 km for the Red Sea margin, <100 km for the Gulf of Aden margin) variation as a lateral transition between a thick crust and a thinned, intruded and stretched crust. In addition, our new seismic images showing lower mantle velocities under the south-western corner of Yemen is consistent with ongoing rifting above a thermal anomaly in the underlying mantle, due to the Afar plume. Under these conditions, melt generated by adiabatic decompression of the asthenosphere beneath thinned and stretched lithosphere migrates upward to intrude or underplate continental crust and extrude as mostly basalt flows (Oligocene flood basalts) [*White and McKenzie*, 1989]. Our positive Vp anomaly near the base of the crust under the Red Sea and Gulf of Aden margin is consistent with melt produced from an abnormally hot mantle which enriches the melt in MgO [*White and McKenzie*, 1989], capable of producing intrusions/underplate of up to 7.2 km/s rather than 6.8 km/s from melting normal mantle. These high-velocity anomalies are focused mainly into narrow zones of denser material, away from the most stretched areas. That is because the mantle temperature was highest at the start of continental breakup [*White et al.*, 2008]. Such lower crustal intrusions/underplating are a common feature of volcanic margins such as the north Atlantic [*Geoffroy*, 2005; *Mjelde et al.*, 2005; *White et al.*, 2008].

Placing constraints on the timing of the underplating is difficult. If emplaced before the eruption of SDRs and continental breakup as has been proposed for the north Atlantic (at least 10–15 Ma off Norway) [*Gernigon et al.*, 2006] then it would have an influence on the structural development of the margin and partly consist of high-pressure granulite/eclogite lower crustal rocks [*Gernigon et al.*, 2006].

At shallower depths of 0–30 km in our model, seismic anomalies are directly related to the geological units observed at the surface. The granitic intrusions of Jabal Hufash and Jabal Bura are associated with high-velocity anomalies (up to +4%, see Figure 2). The depth extent of the anomaly below the granitic intrusions of Jabal Hufash may indicate a deeper root, as hypothesized by *Denèle et al.* [2012]. It could also be explained by a stronger smearing effect due to the high amplitude of the Jabal Hufash anomaly.

### 7.2. Deep Structure of the Margins

Our synthetic tests show that deep anomalies cannot be explained by the smearing in depth of crustal anomalies. We interpret the low-velocity anomaly (−2%) between ∼35 km and 300 km depth under the highest topography as abnormally hot mantle upwelling. This low-velocity hotter mantle is located below the stations DAMY, RUSA, and YSLE (Figure 5), which are located on the thick Oligocene flood basalts and three more recent volcanic fields (15 Ma to present) volcanic areas, e.g., Dhamar and Sana'a [*Davison et al.*, 1994; *Pik et al.*, 2008; *Leroy et al.*, 2010b], see Figure 2. Additionally, we infer presence of partial melt in the crust or uppermost mantle to be responsible for this low-velocity anomaly (Figure 10). A similar pattern of upper mantle off-axis upwelling has also been found in the southern Red Sea rift of Afar and explained by small diapiric upwellings (<100 km) [*Hammond et al.*, 2013]. We surmise that a similar mechanism is the best explanation for our observations. This idea is supported by the large asthenospheric component in the magma from the three Yemeni volcanic fields inferred from trace element and isotope geochemistry [*Manetti et al.*, 1991]. Observations of recent dike intrusions at Harrat Lunayirr in Saudi Arabia [*Pallister et al.*, 2010] show rifted margin magmatism may be important in accommodating extension after breakup along the full length of the Red Sea margin [*Ebinger and Belachew*, 2010].

Our new relative *P* wave velocity model beneath western Yemen suggests the young rift flank volcanoes on the margin of the Red Sea rift are caused by focused small-scale diapiric upwelling from a broad region of hot mantle beneath the area. Our work shows that relatively hot mantle, along with partial melting of the mantle, can persist beneath rifted margins after breakup has occurred. These findings have important implications for interpreting the thermal history and deformation of volcanic rifted margins after breakup is achieved since most breakup models assume rift margin volcanism ceases after seafloor spreading starts.

Buoyant hot mantle may contribute to a dynamic topography of the Yemeni high plateau. Almost all the topography in this region could indeed have a dynamic origin, because the rift-flank uplift from flexure [*Daradich et al.*, 2003] is not sufficient to produce high topographies over such a large area. Numerical modeling of the plume/lithosphere interaction predicts an uplift of about 500–1500 m in less than 0.3–0.5 Ma after the plume initiation [*d'Acremont et al.*, 2003]. Moreover, *White and McKenzie* [1989] explained that an increase of about 150°C in the mantle leads to a dynamic uplift, but that the addition of dense igneous material under a thinned crust produces an immediate subsidence of more than 2 km in order to maintain isostatic equilibrium. We observe a similar pattern on the Red Sea and Gulf of Aden margins, with high Yemeni plateau dynamically supported by a hot mantle (Figures 5a, 5b, and 5d), and a subsiding area, for example, the Tihama Plain, underlained by seaward dipping reflectors and ultramafic bodies accreted under the crust. This hypothesis should however be tested for Yemen by gravity and isostatic modeling.

The weak low-velocity anomaly imaged under the south-western corner of Yemen, beneath the MOKA station, is underneath the Miocene volcanic area of Jabal An Nar. Our synthetic test (Figure 9) shows that this low-velocity anomaly may be explained by a large zone of hotter mantle. This feature could be due to the Afar plume signal, located only ∼300 km away, in the Afar depression.

## 8. Conclusions

We performed an inversion of *P* wave teleseismic data to image lithospheric structure beneath the SW of the Yemen, the southern Red Sea, and western Gulf of Aden margins. The crustal part of the model is dominated by a possible ultramafic underplating beneath the Red Sea and Gulf of Aden margins, a sudden thinning of the crust for this volcanic margin, and Tertiary granitic intrusions (Jabal Hufash and Jabal Bura). In

the mantle, we image a low-velocity anomaly in which we infer partial melting just below the highest topography, the thick Oligocene flood basalts and other off-axis volcanic regions (from 15 Ma to present). This low-velocity anomaly could correspond to an abnormally hot mantle and could be responsible for dynamic topography and recent magmatism in western Yemen. Some hot material has also been inferred under the south-western corner of Yemen and may be due to the Afar plume signal.

## References

Ahmed, A., C. Tiberi, S. Leroy, G. W. Stuart, D. Keir, J. Sholan, K. Khanbari, I. Al-Ganad, and C. Basuyau (2013), Crustal structure of the rifted volcanic margins and uplifted plateau of Western Yemen from receiver function analysis, *Geophys. J. Int.*, *193*(3), 1673–1690.

Aki, K., A. Christofferson, E. Husebye, and C. Powell (1974), Three-dimensional seismic velocity anomalies in the crust and upper-mantle under the USGS, California seismic array, *Eos Trans. AGU*, *56*, 1145.

Aki, K., A. Christoffersson, and E. Husebye (1977), Determination of the three-dimensional seismic structure of the lithosphere, *J. Geophys. Res.*, *82*, 277–296.

Autin, J., S. Leroy, M. Beslier, E. d'Acremont, P. Razin, A. Ribodetti, N. Bellahsen, C. Robin, and K. Al Toubi (2010), Continental break-up history of a deep magma-poor margin based on seismic reflection data (northeastern Gulf of Aden margin, offshore Oman), *Geophys. J. Int.*, *180*(2), 501–519.

Baker, J., L. Snee, and M. Menzies (1996), A brief Oligocene period of flood volcanism in Yemen: Implications for the duration and rate of continental flood volcanism at the Afro-Arabian triple junction, *Earth Planet. Sci. Lett.*, *138*(1), 39–55.

Bastow, I., and D. Keir (2011), The protracted development of the continent-ocean transition in Afar, *Nat. Geosci.*, *4*(4), 248–250.

Bastow, I., G. Stuart, J. Kendall, and C. Ebinger (2005), Upper-mantle seismic structure in a region of incipient continental breakup: Northern Ethiopian Rift, *Geophys. J. Int.*, *162*(2), 479–493.

Bastow, I., D. Keir, and E. Daly (2011), The Ethiopia Afar Geoscientific Lithospheric Experiment (EAGLE): Probing the transition from continental rifting to incipient seafloor spreading, *Volcanism Evol. Afr. Lithosphere*, *478*, 51–76.

Basuyau, C., C. Tiberi, S. Leroy, G. Stuart, A. Al-Lazki, K. Al-Toubi, and C. Ebinger (2010), Evidence of partial melting beneath a continental margin: Case of Dhofar, in the Northeast Gulf of Aden (Sultanate of Oman), *Geophys. J. Int.*, *180*(2), 520–534.

Benoit, M., A. Nyblade, J. VanDecar, and H. Gurrola (2003), Upper mantle P wave velocity structure and transition zone thickness beneath the Arabian Shield, *Geophys. Res. Lett.*, *30*(10), 1531, doi:10.1029/2002GL016436.

Benoit, M., A. Nyblade, and J. VanDecar (2006), Upper mantle P-wave speed variations beneath Ethiopia and the origin of the Afar hotspot, *Geology*, *34*(5), 329–332.

Bertrand, H., G. Chazot, J. Blichert-Toft, and S. Thoral (2003), Implications of widespread high-$\mu$ volcanism on the Arabian Plate for Afar mantle plume and lithosphere composition, *Chem. Geol.*, *198*(1), 47–61.

Boschi, L., T. Becker, and B. Steinberger (2007), Mantle plumes: Dynamic models and seismic images, *Geochem. Geophys. Geosyst.*, *8*, Q10006, doi:10.1029/2007GC001733.

Boschi, L., T. W. Becker, and B. Steinberger (2008), On the statistical significance of correlations between synthetic mantle plumes and tomographic models, *Phys. Earth Planet. Inter.*, *167*(3), 230–238.

Calò, M., C. Dorbath, D. Luzio, S. Rotolo, and G. d'Anna (2008), WAM tomography in the southern Tyrrhenian region. Petrological inferences and hypotheses on the fluid circulation in the subducting Ionian slab and adjoining mantle domain, *Bollettino Geofis. Teorica Appl.*, *42*(2), 136–141.

Chang, S., and S. Van der Lee (2011), Mantle plumes and associated flow beneath Arabia and East Africa, *Earth Planet. Sci. Lett.*, *302*(3-4), 448–454.

Chang, S., M. Merino, S. Van der Lee, S. Stein, and C. Stein (2011), Mantle flow beneath Arabia offset from the opening Red Sea, *Geophys. Res. Lett.*, *38*, L04301, doi:10.1029/2010GL045852.

Coulié, E., X. Quidelleur, P. Gillot, V. Courtillot, J. Lefèvre, and S. Chiesa (2003), Comparative K–Ar and Ar/Ar dating of Ethiopian and Yemenite Oligocene volcanism: Implications for timing and duration of the Ethiopian traps, *Earth Planet. Sci. Lett.*, *206*(3), 477–492.

Courtillot, V., C. Jaupart, I. Manighetti, P. Tapponnier, and J. Besse (1999), On causal links between flood basalts and continental breakup, *Earth Planet. Sci. Lett.*, *166*(3), 177–195.

d'Acremont, E., S. Leroy, and E. Burov (2003), Numerical modelling of a mantle plume: The plume head-lithosphere interaction in the formation of an oceanic large igneous province, *Earth Planet. Sci. Lett.*, *206*(3-4), 379–396.

d'Acremont, E., S. Leroy, M. Maia, P. Gente, and J. Autin (2010), Volcanism, jump and propagation on the Sheba ridge, eastern Gulf of Aden: Segmentation evolution and implications for oceanic accretion processes, *Geophys. J. Int.*, *180*(2), 535–551.

Daradich, A., J. Mitrovica, R. Pysklywec, S. Willett, and A. Forte (2003), Mantle flow, dynamic topography, and rift-flank uplift of Arabia, *Geology*, *31*(10), 901–904.

Davison, I., et al. (1994), Geological evolution of the southeastern Red Sea Rift margin, Republic of Yemen, *Geol. Soc. Am. Bull.*, *106*(11), 1474–1493.

Debayle, E., J. Lévêque, and M. Cara (2001), Seismic evidence for a deeply rooted low-velocity anomaly in the upper mantle beneath the northeastern Afro/Arabian continent, *Earth Planet. Sci. Lett.*, *193*(3), 423–436.

Denèle, Y., R. Pik, and S. Leroy (2012), Thermal and tectonic histories of the Jabel-Bura per-alkaline granite on the south-eastern margin of the Red Sea (Yemen), paper presented at Magmatic Rifting and Active Volcanism Conference, Addis Abeba.

Ebinger, C., and M. Belachew (2010), Geodynamics: Active passive margins, *Nat. Geosci.*, *3*, 670–671.

Ebinger, C., and N. Sleep (1998), Cenozoic magmatism throughout east Africa resulting from impact of a single plume, *Nature*, *395*(6704), 788–791.

El-Anbaawy, M. I. H., M. A. H. Al-Aawah, K. A. Al-Thour, and M. Tucker (1992), Miocene evaporites of the Red Sea Rift, Yemen Republic: Sedimentology of the Salif halite, *Sediment. Geol.*, *81*, 61–71.

Evans, J., and U. Achauer (1993), Teleseismic velocity tomography using the ACH method: Theory and application to continental-scale studies, in *Seismic Tomography Theory and Practice*, pp. 319–360, Chapman and Hall, London.

Forte, A. M., S. Quéré, R. Moucha, N. A. Simmons, S. P. Grand, J. X. Mitrovica, and D. B. Rowley (2010), Joint seismic–geodynamic-mineral physical modelling of African geodynamics: A reconciliation of deep-mantle convection with surface geophysical constraints, *Earth Planet. Sci. Lett.*, *295*(3), 329–341.

Gao, W., S. Grand, W. Baldridge, D. Wilson, M. West, J. Ni, and R. Aster (2004), Upper mantle convection beneath the Central Rio Grande rift imaged by P and S wave tomography, *J. Geophys. Res.*, *109*, BO3305, doi:10.1029/2003JB002743.

Geoffroy, L. (2005), Volcanic passive margins, *C. R. Geosci.*, *337*, 1395–1408.

Geoffroy, L., P. Huchon, and K. Khanbari (2002), Did Yemeni Tertiary granites intrude neck zones of a stretched continental upper crust?, *Terra Nova*, *10*(4), 196–200.

George, R., N. Rogers, and S. Kelley (1998), Earliest magmatism in Ethiopia: Evidence for two mantle plumes in one flood basalt province, *Geology*, *26*(10), 923–926.

Gernigon, L., F. Lucazeau, F. Brigaud, J. Ringenbach, S. Planke, and B. Le Gall (2006), A moderate melting model for the Vøring margin (Norway) based on structural observations and a thermo-kinematical modelling: Implication for the meaning of the lower crustal bodies, *Tectonophysics*, *412*(3), 255–278.

Hammond, J., et al. (2013), Mantle upwelling and initiation of rift segmentation beneath the Afar Depression, *Geology*, *41*(6), 635–638.

Hébert, H., C. Deplus, P. Huchon, K. Khanbari, and L. Audin (2001), Lithospheric structure of the nascent west Gulf of Aden spreading center inferred from gravity data, *J. Geophys. Res.*, *106*, 26,345–26,363.

Hofmann, C., V. Courtillot, G. Féraud, P. Rochette, G. Yirgu, E. Ketefo, and R. Pik (1997), Timing of the Ethiopian flood basalt event and implications for plume birth and global change, *Nature*, *389*, 838–841.

Jordan, M., and U. Achauer (1999), A new method for the 3-D joint inversion of teleseismic delaytimes and Bouguer gravity data with application to the French Massif Central, *EOS Trans. AGU*, *80*(46), Fall Meet. Suppl.

Karato, S. (1993), Importance of anelasticity in the interpretation of seismic tomography, *Geophys. Res. Lett.*, *20*, 1623–1626.

Kennett, B., and E. Engdahl (1991), Traveltimes from global earthquake location and phase identification, *Geophys. J. Int.*, *105*, 429–465.

Koulakov, I. (2011), High-frequency P and S velocity anomalies in the upper mantle beneath Asia from inversion of worldwide traveltime data, *J. Geophys. Res.*, *116*, B04301, doi:10.1029/2010JB007938.

Leroy, S., E. d'Acremont, C. Tiberi, C. Basuyau, J. Autin, F. Lucazeau, and H. Sloan (2010a), Recent off-axis volcanism in the eastern Gulf of Aden: Implications for plume–ridge interaction, *Earth Planet. Sci. Lett.*, *293*(1), 140–153.

Leroy, S., et al. (2010b), Contrasted styles of rifting in the eastern Gulf of Aden: A combined wide-angle, multichannel seismic, and heat flow survey, *Geochem. Geophys. Geosyst.*, *11*, Q07004, doi:10.1029/2009GC002963.

Leroy, S., et al. (2012), From rifting to oceanic spreading in the Gulf of Aden: A synthesis, *Arabian J. Geosci.*, *5*, 859–901.

Lucazeau, F., et al. (2009), Post-rift volcanism and high heat-flow at the ocean-continent transition of the eastern Gulf of Aden, *Terra Nova*, *21*(4), 285–292.

Manetti, P., G. Capaldi, S. Chiesa, L. Civetta, S. Conticelli, M. Gasparon, L. Volpe, and G. Orsi (1991), Magmatism of the eastern Red Sea margin in the northern part of Yemen from Oligocene to present, *Tectonophysics*, *198*(2), 181–202.

Martin, M., and J. Ritter (2005), High-resolution teleseismic body-wave tomography beneath SE Romania–I. Implications for three-dimensional versus one-dimensional crustal correction strategies with a new crustal velocity model, *Geophys. J. Int.*, *162*(2), 448–460.

Mechie, J., Z. Ben-Avraham, M. Weber, H.-J. Götze, I. Koulakov, A. Mohsen, and M. Stiller (2013), The distribution of Moho depths beneath the Arabian plate and margins, *Tectonophysics*, *609*, 234–249, doi:10.1016/j.tecto.2012.11.015.

Mjelde, R., T. Raum, B. Myhren, H. Shimamura, Y. Murai, T. Takanami, R. Karpuz, and U. Næss (2005), Continent-ocean transition on the Vøring Plateau, NE Atlantic, derived from densely sampled ocean bottom seismometer data, *J. Geophys. Res.*, *110*, B05101, doi:10.1029/2004JB003026.

Montagner, J., et al. (2007), Mantle upwellings and convective instabilities revealed by seismic tomography and helium isotope geochemistry beneath eastern Africa, *Geophys. Res. Lett.*, *34*, L21303, doi:10.1029/2007GL031098.

Montelli, R., G. Nolet, F. Dahlen, and G. Masters (2006), A catalogue of deep mantle plumes: New results from finite-frequency tomography, *Geochem. Geophys. Geosyst*, *7*, Q11007, doi:10.1029/2006GC001248.

Moucha, R., and A. M. Forte (2011), Changes in African topography driven by mantle convection, *Nat. Geosci.*, *4*(10), 707–712.

Pallister, J., et al. (2010), Broad accommodation of rift-related extension recorded by dyke intrusion in Saudi Arabia, *Nat. Geosci.*, *3*(10), 705–712.

Pik, R., B. Marty, J. Carignan, G. Yirgu, and T. Ayalew (2008), Timing of East African Rift development in southern Ethiopia: Implication for mantle plume activity and evolution of topography, *Geology*, *36*(2), 167–170.

Rolandone, F., F. Lucazeau, S. Leroy, J.-C. Mareschal, R. Jorand, B. Goutorbe, and H. Bouquerel (2013), New heat flow measurements in Oman and the thermal state of the Arabian Shield and Platform, *Tectonophysics*, *589*, 77–89.

Rooney, T., C. Herzberg, and I. Bastow (2012), Elevated mantle temperature beneath East Africa, *Geology*, *40*(1), 27–30.

Sebai, A., E. Stutzmann, J. Montagner, D. Sicilia, and E. Beucler (2006), Anisotropic structure of the African upper mantle from Rayleigh and Love wave tomography, *Phys. Earth Planet. Inter.*, *155*(1), 48–62.

Sicilia, D., et al. (2008), Upper mantle structure of shear-waves velocities and stratification of anisotropy in the Afar Hotspot region, *Tectonophysics*, *462*(1-4), 164–177.

Sobolev, S. V., H. Zeyen, G. Stoll, F. Werling, R. Altherr, and K. Fuchs (1996), Upper mantle temperatures from teleseismic tomography of French Massif Central including effects of composition, mineral reactions, anharmonicity, anelasticity and partial melt, *Earth Planet. Sci. Lett.*, *139*(1), 147–163.

Tard, F., P. Masse, F. Walgenwitz, and P. Gruneisen (1991), The volcanic passive margin in the vicinity of Aden, Yemen, *Bull. Cent. Rech. Explor. Prod. Elf Aquitaine*, *15*, 1–9.

Thurber, C. H. (1983), Earthquake locations and three-dimensional crustal structure in the Coyote Lake Area, central California, *J. Geophys. Res.*, *88*, 8226–8236, doi:10.1029/JB088iB10p08226.

Tiberi, C., A. Deschamps, J. Déverchère, C. Petit, J. Perrot, D. Appriou, V. Mordvinova, T. Dugaarma, M. Ulzibaat, and A. Artemiev (2008), Asthenospheric imprints on the lithosphere in Central Mongolia and Southern Siberia from a joint inversion of gravity and seismology (MOBAL experiment), *Geophys. J. Int.*, *175*(3), 1283–1297.

Watremez, L., S. Leroy, S. Rouzo, E. d'Acremont, P. Unternehr, C. Ebinger, F. Lucazeau, and A. Al-Lazki (2011), The crustal structure of the north-eastern Gulf of Aden continental margin: Insights from wide-angle seismic data, *Geophys. J. Int.*, *184*(2), 575–594.

Weiland, C., L. Steck, P. Dawson, and V. Korneev (1995), Nonlinear teleseismic tomography at Long Valley caldera, using three-dimensional minimum travel time ray tracing, *J. Geophys. Res.*, *100*, 20,379–20,390.

White, R., and D. McKenzie (1989), Magmatism at rift zones: The generation of volcanic continental margins and flood basalts, *J. Geophys. Res.*, *94*, 7685–7729.

White, R., et al. (2008), Lower-crustal intrusion on the North Atlantic continental margin, *Nature*, *452*(7186), 460–464.

Zeyen, H., and U. Achauer (1997), Joint inversion of teleseismic delay times and gravity anomaly data for regional structures. Theory and synthetic examples, *NATO ASI Ser., Ser. 1*, *17*, 155–168.

Zhao, D. (2007), Seismic images under 60 hotspots: Search for mantle plumes, *Gondwana Res.*, *12*(4), 335–355.

Zhao, D., A. Hasegawa, and H. Kanamori (1994), Deep structure of Japan subduction zone as derived from local, regional, and teleseismic events, *J. Geophys. Res.*, *99*, 22,313–22,329.

Zhao, D., J. Lei, T. Inoue, A. Yamada, and S. S. Gao (2006), Deep structure and origin of the Baikal rift zone, *Earth Planet. Sci. Lett.*, *243*(3), 681–691.

Zumbo, V., G. Féraud, H. Bertrand, and G. Chazot (1995), 40Ar/39Ar chronology of Tertiary magmatic activity in Southern Yemen during the early Red Sea-Aden Rifting, *J. Volcanol. Geotherm. Res.*, *65*(3-4), 265–279.